More than just a line: Shining light on the flattening radial metallicity gradient of a NIHAO Milky-Way analogue simulation

S. Buder,[1,2]★ and T. Buck,[3,4]
[1]Research School of Astronomy & Astrophysics, Australian National University, ACT 2611, Australia
[2]Center of Excellence for Astrophysics in Three Dimensions (ASTRO-3D), Australia
[3]Universität Heidelberg, Interdisziplinäres Zentrum für Wissenschaftliches Rechnen, Im Neuenheimer Feld 205, D-69120 Heidelberg, Germany
[4]Universität Heidelberg, Zentrum für Astronomie, Institut für Theoretische Astrophysik, Albert-Ueberle-Straße 2, D-69120 Heidelberg, Germany

Accepted YYYY Month DD. Received YYYY Month DD

ABSTRACT
Radial metallicity gradients in galaxies are crucial for understanding the processes of galactic formation and its dynamical and chemical evolution. We use young stars and gas of a high-resolution simulation of a NIHAO Milky Way analogue galaxy to analyse four properties of the radial metallicity gradient, namely its linearity and scatter as well as its coherence with radial coverage, azimuth, and age. While a global linear fit with slope traces the gradient well, we find it to be too flat in the inner galaxy and too steep in the outer galaxy. An initially stepper but then flattening second order quadratic function provides a superior fit down to the smallest radial steps, where less regular effects take over. We identify these as SB: spiral arms or warp? when tracing them across the Galactic position. The simulation further exhibits a steadily increasing spread in [Fe/H] even among the young stars from 0.01 dex in the inner galaxy to 0.14 dex in at a radius 20 kpc coinciding with decreasing stellar density and increased flaring of stars towards higher heights with little correlation across the small age range of 1 Gyr. We conclude that future Galactic and extragalactic observational studies should test our theoretical prediction of a quadratic gradient function with their data to confirm or reject previous observational claims of a broken linear radial metallicity gradients proposed for the Milky Way and other spiral galaxies, as either function implies different dynamical and chemical galaxy formation and evolution scenarios.

Key words: cosmology: observations – Galaxy: structure – Galaxy: abundances – galaxies: structure – galaxies: abundances

1 INTRODUCTION

Radial metallicity gradients in galaxies, defined as the change in metal abundance with galactocentric radius, offer vital insights into the processes that shape the chemical and dynamical evolution of galaxies. The decrease in metallicity with increasing distance from the Galactic center is well-established both theoretically (Larson 1976; Tinsley 1980; Chiosi 1980) and observationally in the Milky Way (Searle 1971; Janes 1979; Twarog et al. 1997). However, the specific shape and characteristics of this gradient remain somewhat unclear.

The Milky Way, being the only galaxy where we can resolve millions of stars, provides a unique opportunity to study these gradients in detail. Over two decades ago, Chiappini (2002) highlighted the contradictions in the observed shape, magnitude, and evolution of abundance gradients. Recent advancements, such as the *Gaia* mission (Gaia Collaboration et al. 2016), have significantly expanded our observational data, allowing for more detailed studies of these gradients.

For instance, Hogg et al. (2019) created an extensive metallicity map of the Milky Way using APOGEE and *Gaia* data, while Poggio et al. (2022) mapped young stars and found a metallicity excess around spiral arms (see also Zari et al. 2018, 2021; Poggio et al. 2021; Hackshaw et al. 2024). Similarly, Imig et al. (2023, among others) traced gradients across different stellar populations and ages, emphasizing the importance of considering radial migration effects (Binney & Tremaine 2008; Frankel et al. 2018, 2020).

Historically, radial metallicity gradients have been measured using various stellar populations and gas tracers. Early evidence by Janes (1979) suggested a gradient on the order of

$$\frac{\mathrm{d[Fe/H]}}{\mathrm{d}R} = -0.05 \pm 0.01, \mathrm{dex}, \mathrm{kpc}^{-1} \quad (1)$$

for the Milky Way which aligns with more recent measurements (Anders et al. 2017; Hayden et al. 2015). Estimated gradients also seem to be broadly consistent across different stellar tracers, such as young open clusters (e.g. Cunha et al. 2016; Magrini et al. 2017; Casamiquela et al. 2019; Donor et al. 2020; Spina et al. 2021; Myers et al. 2022), young hot (OB-type) stars (Zari et al. 2018, 2021; Poggio et al. 2021, 2022), field stars close to the Galactic plane (e.g. Bergemann et al. 2014) or Cepheids (Andrievsky et al. 2002a,b; Lemasle et al. 2007, 2013). However, these gradients are accompanied by significant spread in [Fe/H] of 0.1 − 0.15 dex, as noted by Twarog (1980), which may imply a fine structure of the metallicity gradient (see Genovali et al. 2014).

Despite extensive observational efforts, several challenges persist:

- The completeness (or patchiness) of observed datasets remains a fundamental issue (Bergemann et al. 2014).
- How robustly can we use the incomplete data to predict substructure in the gradients, such as the need to actually fit two linear

★ E-mail: sven.buder@anu.edu.au

gradients with a break radius at corotation radius (Bresolin et al. 2012, and references therein) or further out (Donor et al. 2020) - or even more complicated functions (see e.g. Chiappini et al. 2001; Kubryk et al. 2015)?

• Different samples yield varying gradients, potentially due to biases in data or the inclusion of older stars (e.g. Boeche et al. 2013; Allende Prieto et al. 2006; Katz et al. 2011; Hayden et al. 2014; Anders et al. 2014; Vickers et al. 2021; Willett et al. 2023).

• The impact of spiral arm structures (Poggio et al. 2021), the Galactic warp (Lemasle et al. 2022) or bar-driven mixing (Di Matteo et al. 2013) on metallicity gradients is not fully understood.

• Methodologies for fitting linear models to scattered data need re-evaluation (Metha et al. 2021).

Understanding these gradients in the Milky Way is also crucial for extragalactic studies, where spatial resolution limits observations. New instruments like the MUSE integral field spectrograph has enabled a plethora of extragalactic studies to contrast the Milky Way to and techniques like the spectroscopy of HII regions and planetary nebulae have helped to infer gas metallicity distributions in external galaxies (Shaver et al. 1983; Vilchez & Esteban 1996; Rolleston et al. 2000; Bresolin et al. 2012). Recent examples include Sánchez et al. (2014) with CALIFA galaxy observations as well as Mun et al. (2024) and Chen et al. (2024) who use MAGPI galaxy observations to probe for example the effects of spiral arms. Notable is also the scatter that Chen et al. (2023) found for the gas metallicity across galactic radius with TYPHOON observations (see their. Figs. 4-6).

From a modelling perspective, galactic chemical evolution models can both test understanding of radial metallicity gradients and make predictions beyond the limited volumes and tracers tested by Milky Way and extragalactic studies. Such galactic chemical evolution models include Chiappini et al. (2001); Minchev et al. (2014); Kubryk et al. (2015); Stanghellini et al. (2015); Matteucci (2001).

New suites of large-scale simulations now allow to gain insights into radial metallicity gradients across a range of simulated galaxies - including Milky Way analogues. While Pilkington et al. (2012) found that such gradients are established by inside-out formation in RaDES simulations, whereas Tissera et al. (2019) used EAGLE simulations to study gradients across different galaxy characteristics, such as mergers and stellar mass. Bellardini et al. (2021) and Bellardini et al. (2022); Graf et al. (2024) compared the radial metallicity gradient and its azimuthal scatter for different simulations of the FIRE suite for gas and stars, respectively. Focusing on the change of the radial metallicity gradient over time, Grand et al. (2015) assessed the scatter of radial metallicity distribution for different stellar ages. Both Ma et al. (2017, see their Fig. 6) with FIRE and Agertz et al. (see their Fig. 9 2021) with VINTERGATAN further assessed the evolution of the radial metallicity gradient for gas and stars. Khoperskov et al. (2023) again focused on the gas and found the scatter of the gas metallicity of $\approx 0.04 - 0.06$ dex at a given galactocentric distance.

This study aims to advance these theoretical insight by addressing four critical scientific questions using a high-resolution simulation of a Milky Way analogue galaxy:

(i) *Linearity of the gradient:* Assess the extent to which the radial metallicity gradient of young stars is linear.

(ii) *Scatter in the gradient:* Quantify the expected scatter in the radial metallicity gradient of young stars.

(iii) *Coherence of the gradient with position:* Investigate the gradient's variation with radial coverage and azimuth.

(iv) *Coherence of the gradient with age:* Determine the reliability of stars as tracers of the gas disk over different ages.

The paper is structured as follows: Section 2 describes the data of our Milky Way analogue NIHAO simulation. Section 3 analyses the radial metallicity gradients of the simulation under the four aforementioned questions. Section 4 discusses them individually and Section 5 bundles them into an overarching conclusion.

2 DATA: A NIHAO MILKY WAY ANALOGUE SIMULATION

For this project, we use a cosmological zoom-in simulation of a Milky Way analogue (`g8.26e11`) from the *Numerical Investigation of a Hundred Astronomical Objects* (NIHAO, Wang et al. 2015). The model volume has a total mass (gas, stars and dark matter) of $8.26 \cdot 10^{11}\,\mathrm{M}_\odot$ and contains $4 \cdot 10^{10}\,\mathrm{M}_\odot$ stellar mass with a stellar mass resolution of $1.06 \cdot 10^5\,\mathrm{M}_\odot$ (Buck et al. 2021) and was calculated as part of the NIHAO-UHD project (Buck et al. 2020).

Simulations were carried out with the smoothed particle hydrodynamics code `Gasoline2` (Wadsley et al. 2017) using cosmological parameters from Planck Collaboration et al. (2014) with initial conditions and energetic feedback descriptions from the NIHAO project (Wang et al. 2015). Zoom-in simulations were then performed as described in detail by Buck et al. (2021) with star formation following Stinson et al. (2006) and energetic feedback following Stinson et al. (2013).

Because computational resources still limit the mass resolution of simulations, we are relying on tracer particles that represent simple stellar populations (SSPs) with the same age, overall metallicity and discrete initial mass function (IMF). Buck et al. (2021) have implemented the flexible chemical evolution code CHEMPY (Rybizki et al. 2017) to calculate the chemical yields for the SSPs. In particular, we use the alternative (`alt`) setup of CHEMPY that assumes a Chabrier (2003) IMF with high-mass slope of $\alpha_\mathrm{IMF} = -2.3$ over a mass range of $0.1 - 100\,\mathrm{M}_\odot$ for SSPs across a metallicity range of $Z/Z_\odot \in [10^{-5}, 2]$. The code calculates the contribution from asymptotic giant branch (AGB) stars, CCSN across a mass range of $8 - 40\,\mathrm{M}_\odot$, and SNIa with a an exponential function with exponent -1.12, a delay time of 40 Myr, and a normalization of the SNI rate of -2.9. For each of these nucleosynthetic channels, yields from the following studies are used: Limongi & Chieffi (2018) for CCSN, Seitenzahl et al. (2013) for SNIa, and Karakas & Lugaro (2016) for AGB stars. Contrary to a previous study by Buder et al. (2024), we take the elemental abundances at face value and do not apply any shifts.

For this project, we limit the simulation data to the main halo by applying PYNBODY's implementation of the Amiga Halo Finder (Knollmann & Knebe 2009) and then reposition and rotate this main halo to be face-on based on the angular momentum with PYNBODY's ANALYSIS.ANGMOM.FACEON module (Pontzen et al. 2013). The main halo has a total half mass radius of 66.0 kpc for all matter and a stellar half mass radius 2.4 kpc. We then further transform the resulting galactocentric Cartesian coordinate (X, Y, Z) and velocities (V_X, V_Y, V_Z) to Cylindrical ones as done in a previous study of this main halo by Buder et al. (2024).

To achieve a roughly similar selection as the observational data of the Milky Way (Genovali et al. 2014) and other galaxies (e.g. Chen et al. 2023), we restrict the simulation data to a galactocentric radius of $R_\mathrm{Gal} \leq 20$ kpc, as shown in Fig. 1. Similar to the Milky Way (Poggio et al. 2018; Lemasle et al. 2022), we note a warp of the stellar and gaseous disk (see Figs. 1b and 1e, respectively).

To avoid too strong effects of radial migration (Binney & Tremaine 2008; Frankel et al. 2018) we further enforce stars to be younger than

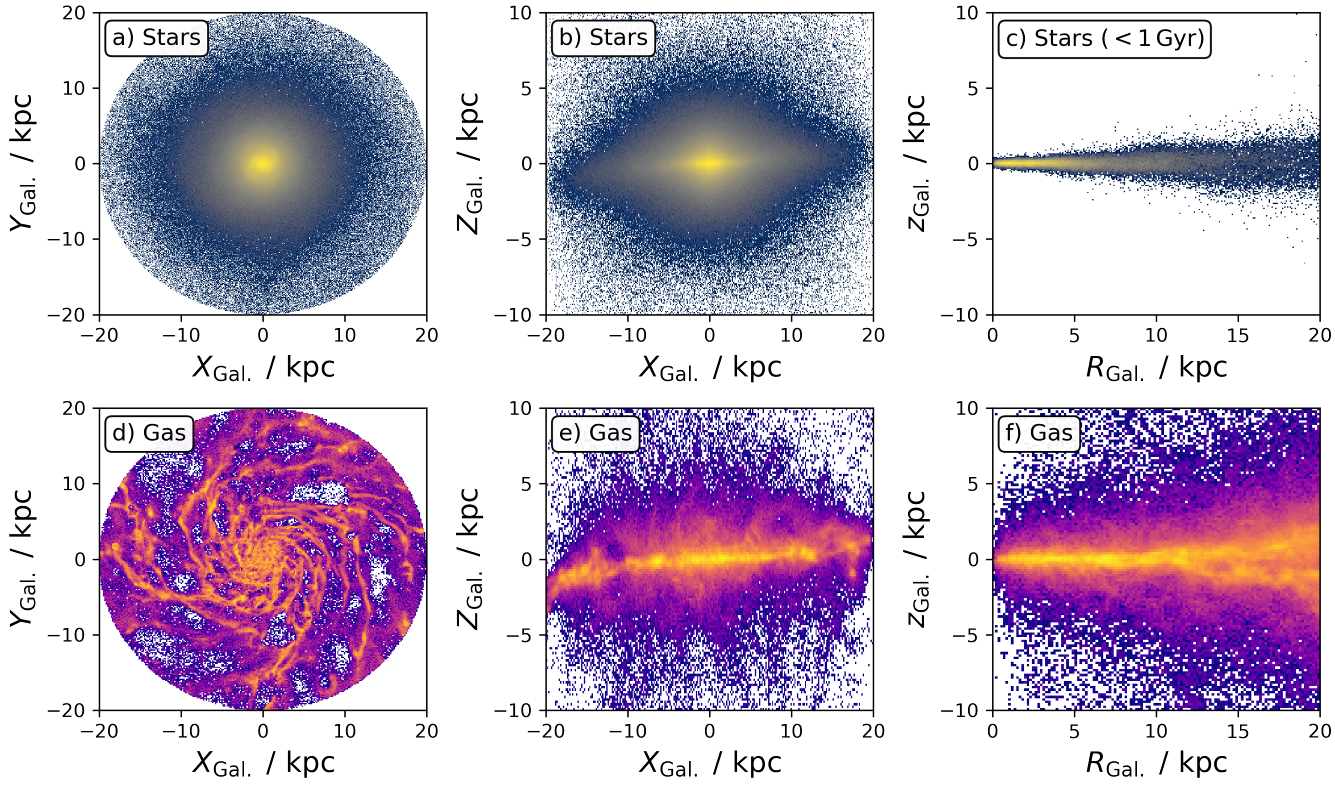

Figure 1. Logarithmic spatial density distribution of stars (upper panels) and gas (lower panels) within $R < 20$ kpc of the NIHAO Milky Way analogue `g8.26e11` in galactocentric cartesian and cylindric coordinates. Panel c) shows the influence of selecting only young stars with ages below 1 Gyr.

1 Gyr. This selection de-facto limits the vertical range of 99% of stars to $|z| = 1.6$ kpc. The strong influence of this age cut on the vertical distribution of stars in the Milky Way analogue can best be appreciated from the difference of vertical density distributions of stars in Figs. 1b and 1c. We are applying these cuts for all following analyses of the radial metallicity gradient in Section 3.

3 THE RADIAL METALLICITY GRADIENT IN NIHAO

In our analysis, we follow the structure laid out with the scientific questions in Section 1. In Section 3.1 we assess the linearity of the radial metallicity gradient on a global scale. In Section 3.2 we quantify the scatter of the gradient. In Secs. 3.3 and 3.4 we analyse the coherence of the gradient with position and stellar age, respectively.

3.1 Linearity of the gradient

We show the logarithmic density distribution of star particle iron abundances [Fe/H] across different galactocentric radii $R_{\mathrm{Gal.}}$ in Fig. 2a. This distribution strongly suggests that gradient is predominantly linear, similar to findings of the Milky Way.

The completeness and amount of data points on a global scale allows us, however, to probe this linearity (or more complex behaviour) in more details.

Table 1. Global linear gradient fit results with different methods. LinearRegression is part of the sklearn package.

Method	Intercept ($a_0 \pm \sigma_{a_0}$)	Slope ($a_1 \pm \sigma_{a_1}$)
statsmodels.api.ODR	0.46229 ± 0.00033	-0.04114 ± 0.00004
scipy.odr	0.46232 ± 0.00033	-0.04114 ± 0.00004
np.polyfit	0.46229 ± 0.00033	-0.04114 ± 0.00004
LinearRegression	0.46236 ± 0.00027	-0.04115 ± 0.00007

3.1.1 Global gradient fits

Based on our visual inspection of Fig. 2a, we first fit a global linear radial metallicity gradient to the data. We report the gradient when using using the LinearRegression module of sklearn.linear_model (Pedregosa et al. 2011) in Fig. 2a as red dashed line, but have confirmed this result within the fitting uncertainties with other fitting methods (see Table 1).

We show the fit residuals in Fig. 2b as density distribution as well as in Fig. 2c as percentile distributions in radial bins of $\Delta R_{\mathrm{Gal}} = 0.5$ kpc. While the density distribution shows a lot of substructure, that we will investigate later, we note increase of the median residuals in Fig. 2c towards inner and outer radii, especially for $R_{\mathrm{Gal.}} > 17$ kpc, suggesting a non-linear component to the gradient, which we will follow up in Section 3.1.3.

3.1.2 The impact of radial coverage on linear fits

While we have gained a useful insight into the global function, observational data will rarely cover the full extend of the stellar disk. Using smaller ranges, observational studies have found hints of piece-wise

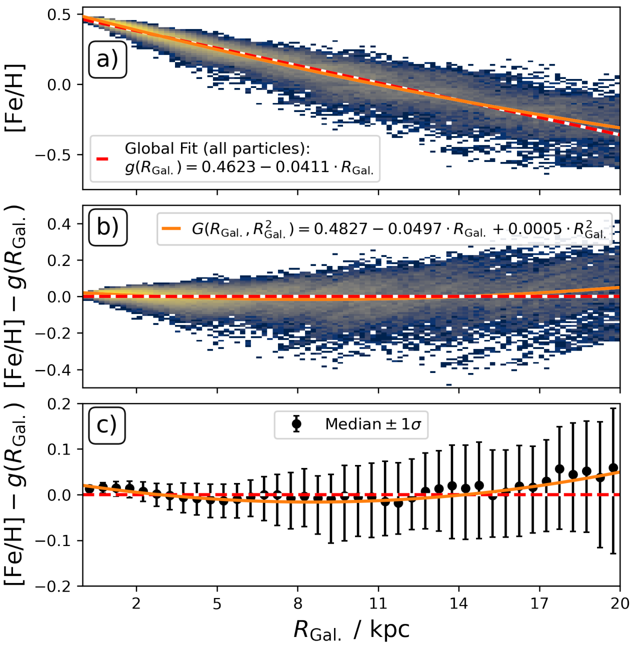

Figure 2. Global fits and deviation to the radial metallicity gradient R – [Fe/H]. Functional forms of the linear (red) and quadratic (orange) lines are shown in the legend. Panel a) shows the underlying data of all data points as logarithmic density and the global fit to them as red dashed line. Panel b) shows the deviation of data from a linear gradient as logarithmic density plot, whereas panel c) shows the 16th and 84th percentile around the median deviation as error bars in $\Delta R_{\rm Gal} = 0.5\,{\rm kpc}$ bins.

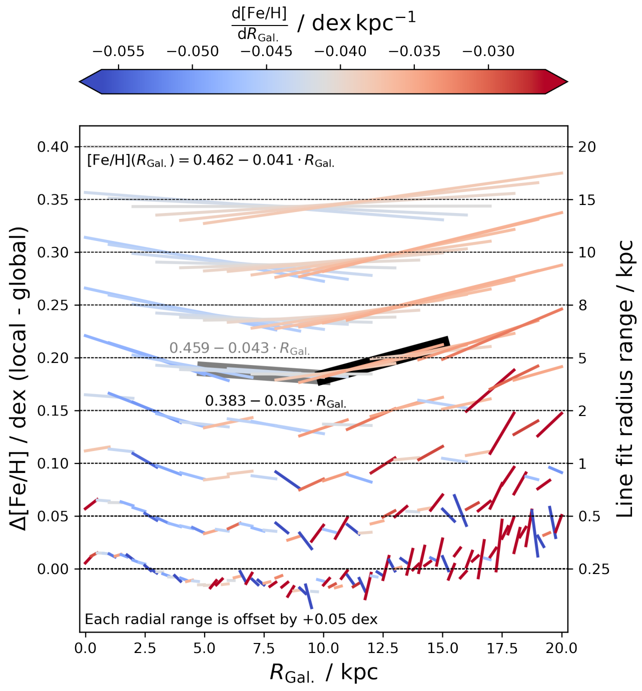

Figure 3. Impact of different coverage in galactocentric radius when fitting a linear radial metallicity gradient to young stars. Each horizontal segment is using a different running radial fitting range between 0.25 and 15 kpc as outlined on the right. For better contrast, the global linear fit is subtracted from the local gradient estimates and each line is colored by the gradient slope with a color scale centered around the global fit slope.

linear gradients with a break radius in them based on a limited radial coverage (e.g. Donor et al. 2020; Chen et al. 2023).

These results are intriguing, since a quadratic function can to first order be approximated by two linear functions with a break radius. We therefore want to use this simulation to test if the radial coverage may indeed delude us into identifying broken linear gradients.

For this purpose, we are fitting and comparing linear radial metallicity gradients to subsets in galactocentric radius. We test fits across piecewise linear radial ranges of 0.25, 0.5, 1, 2, 5, 8, 10, 15, and 20 kpc and show their difference with respect to a global linear fit in Fig. 3, with color-coding and indicating the local gradient slope. In this figure, a horizontal line indicates the same slope as the global fit, whereas the offset of a line from the horizontal dashed line indicates the local deviation from the global gradient. We see that all ranges do suggest more or less significant deviations from a global linear fit, with the innermost fit suggesting a significantly different gradient than the outermost fit. We also note increasingly more slope differences towards the smallest scales, hinting at local deviations from a global pattern. We follow these up in Section 3.2, but for now focus on the larger-scale trends.

When directly comparing an inner and outer radius fit, such as between $R_{\rm Gal.} = 5\text{–}10\,{\rm kpc}$ (thick grey line in Fig. 3) and $R_{\rm Gal.} = 10\text{–}15\,{\rm kpc}$ (thick black line in Fig. 3), we note a significant change, similar to previous estimates of the Milky Way (e.g. Lemasle et al. 2008). In our case the gradient estimate changes from $[{\rm Fe/H}](R_{\rm Gal.}) = 0.459 - 0.043 \cdot R_{\rm Gal.}$ to $[{\rm Fe/H}](R_{\rm Gal.}) = 0.383 - 0.035 \cdot R_{\rm Gal.}$.

3.1.3 *Higher-order gradients*

From the previous section, and especially the changing deviation of local gradients from a global fit in Fig. 3, we acknowledge that a linear fit is - not unexpected - not able to capture the more intricate details of the radial abundance gradient. In particular, we realise that the abundance gradient is indeed flattening - even for stars with young ages (< 1 Gyr). When looking at linear gradient fits across radial coverages of $\Delta R_{\rm Gal.} = 5 - 15\,{\rm kpc}$ in Fig. 3, the gradient was steeper (bluer color) for smaller radii and flatter (redder) for larger radii.

While such effects have seen before for the Milky Way, previous studies how mostly suggested to fit piecewise linear gradients with a break radius (e.g. Andrievsky et al. 2002a; Boeche et al. 2013; Hayden et al. 2014; Anders et al. 2017; Donor et al. 2020).

Our results from Fig. 3 suggest, however, not one break radius, but rather an smoothly evolving flattening, in better agreement with a quadratic function rather than two linear ones. In this section, we are therefore trying to expand the gradient function by a higher order, that is second order, one.

A quadratic fit (see orange lines in Fig. 2) results in a slightly steeper linear component of the gradient (from −0.0411 to −0.0497 dex kpc^{-1}), which is counteracted by the quadratic flattening term of +0.0005 dex kpc^{-2}. The latter leads to an effective flattening of 0.2 dex at $R_{\rm Gal.} = 20\,{\rm dex}$. While seemingly only a nuisance correction across the large extend of [Fe/H] and $R_{\rm Gal.}$, this quadratic function is in fact superior to the linear fit. This can be best appreciated in Fig. 2c, where the orange line is tracing the median residuals from the linear function much better across the all radii.

When reproducing the local deviations from the linear global fit

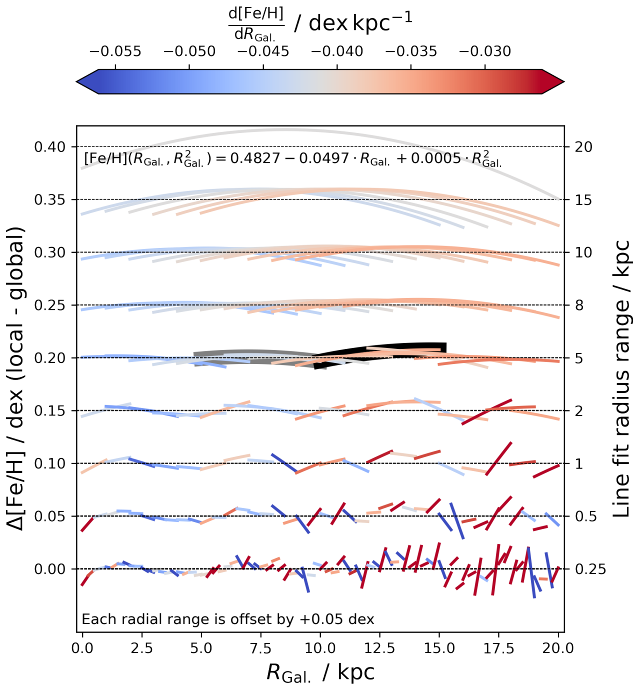

Figure 4. Same as Fig. 3, but comparing local deviations to a quadratic global fit. Overall deviations have decreased most notably for innermost and outermost radii.

(Fig. 3) with a quadratic global fit (Fig. 4), we see that the deviations of the local fits no longer have significant offsets with respect to the horizontal lines, while still showing the increasing slope differences at the local levels (especially on scales below 1 kpc).

3.2 Scatter and local deviations from the gradient

Now that we are sufficiently satisfied that our flattening linear gradient reproduces the overall shape of the radial metallicity gradient, we SB: CONTINUE

see Fig. 5 -> maybe something to do with gas density and or logal variations of gas? should we maybe also plot the star positions here to check for differences or $R - z$ for stars? YES!

SB: How significant is the difference of linear to quadratic when looking at 5-19 kpc, like MW studies (Genovali et al. 2014)?

Motivated by the significant spread of open cluster metallicities at the solar radius beyond observational uncertainty (e.g. Donor et al. 2020; Spina et al. 2021), we are now turning to the scatter of the radial metallicity gradient.

In this section, we investigate

- the change of scatter from the innermost radii to the outermost (see Fig. 2c). We see a steady increase in $1-\sigma$ spread of σ[Fe/H] = 0.01 dex at $R_\mathrm{Gal.} = 0.25 \pm 0.25$ kpc, σ[Fe/H] = 0.06 dex at $R_\mathrm{Gal.} = 8.25 \pm 0.25$ kpc, to σ[Fe/H] = 0.14 dex at $R_\mathrm{Gal.} = 19.5 \pm 0.25$ kpc.

Do the young stars actually trace the gas? See Fig. 6

3.3 Coherence of the gradient with position

- Density variation of the radial metallicity gradient R − [Fe/H] across 8 different sectors in Fig. 7

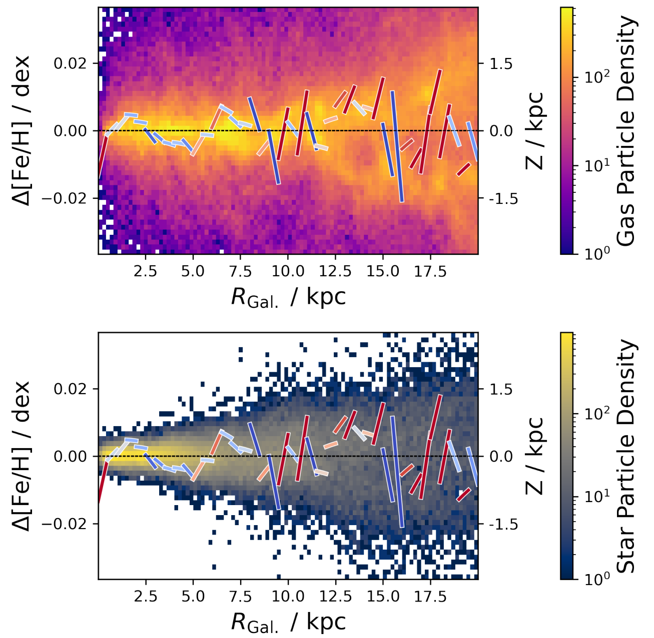

Figure 5. Local gradient deviations from bottom row of Fig. 4 overlapped on the logarithmic density distribution of gas in $R - z$.

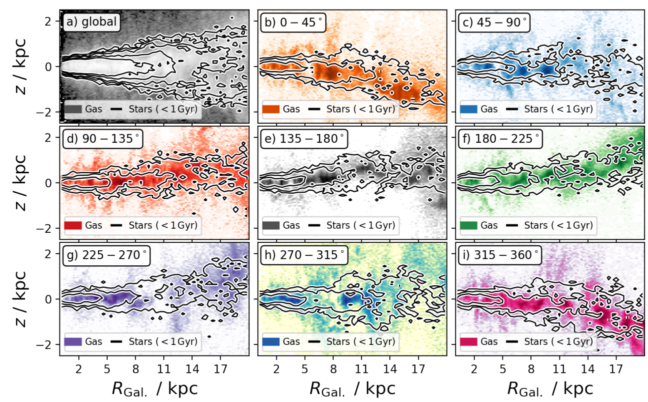

Figure 6. Tracing young stars and gas across the galaxy (panel a) and different azimuthal ranges (panels b-i).

- Deviation from global radial metallicity gradient across 8 different sectors in Fig. 8
- Compute gradient over a radius R and then plot this one in color in the xy direction (like hogg/eilers). Maybe 2kpc is the best radius to do that? Can also try 5kpc.

3.4 Coherence of the gradient with age

SB: Do the same as Fig. 7, but with bins colored by median age.

SB: Global R − [Fe/H], then local for the 8 sectors of Fig. 7, plot both in 2x4 subpanels, and color-code the density plots by median deviation from this line with a seismic map.

SB: see also scatter across age in Fig. 9

The maximum scatter in radius bins varies between 0.073 dex and 0.195 dex across the 0..0.1..1.0 Gyr bins.

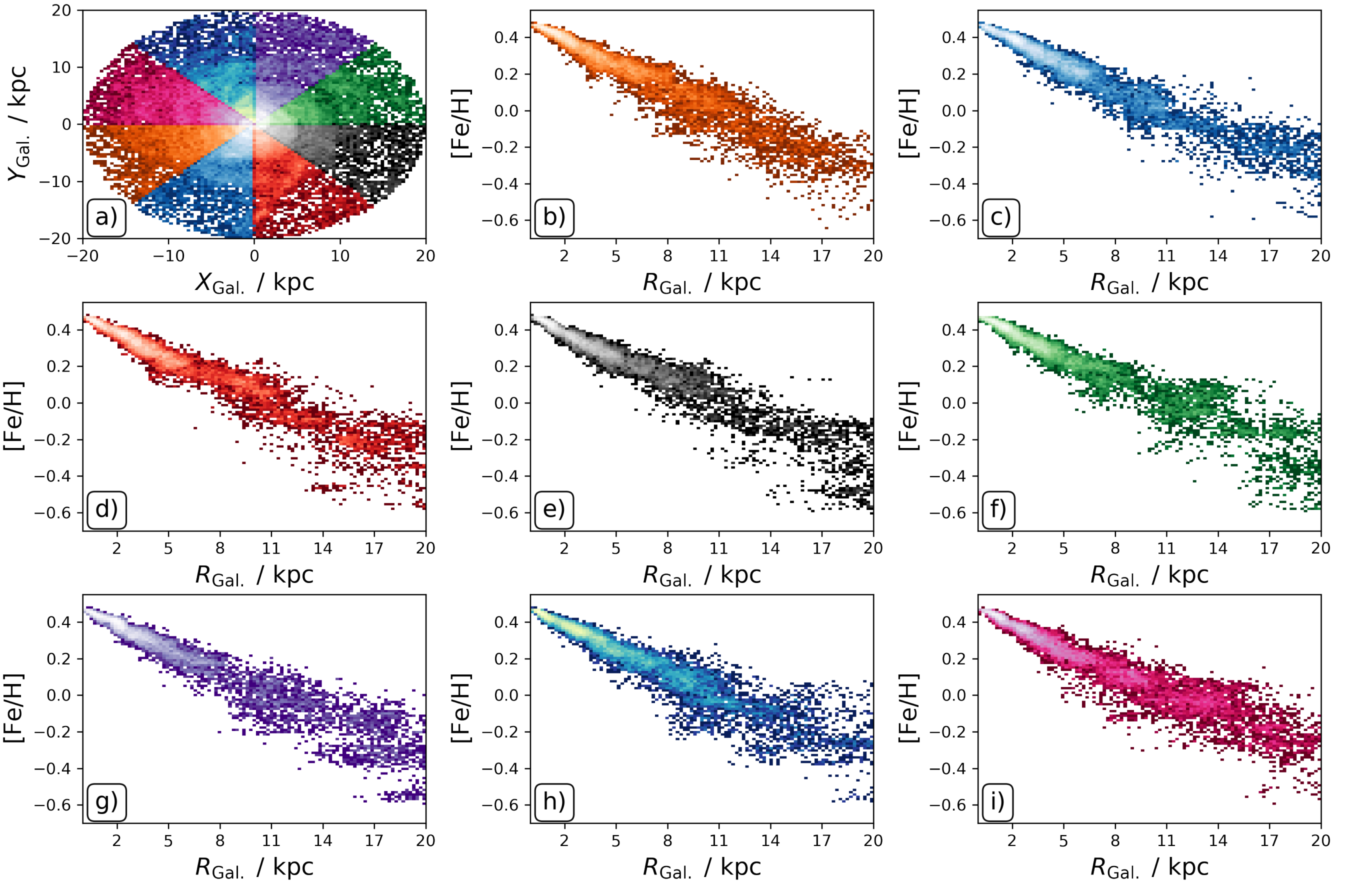

Figure 7. Density variation across 8 different sectors (with color-code visualised in panel a) of the radial metallicity gradient R − [Fe/H] across 8 different azimuth ranges (panels b-i). A rotating lighthouse-like GIF animation of the median age and median density of the R − [Fe/H]-relation is freely available on the github repository.

Fig. 8f shows impressively, that if you look at a rather narrow range of R_{gal}, such as $7 < R_{\mathrm{gal}} < 13$ kpc, the radial metallicity gradient could actually look like it is damping towards larger radii. SB: Is this possibly what is happening in local studies of our galaxy, where many researchers are actually fitting 2 linear gradients with a break radius?

SB: Actually one can see this effect even better in Fig. 7b,d,e,f,h and i!

4 DISCUSSION

Comparison to Minchev et al. (2014, see their Fig. 10): They see significant decrease of stars towards larger radii (note to myself: their bins are not scatter, but number density in Fig. 10). How does this compare to our number densities?

4.1 Linearity of the gradient

SB: How are the linear metallicity gradients usually measured? Any binning? If so, can we study what effect that has? How are uncertainties treated?

To what extent is the radial metallicity gradient of young stars linear? Alternatively, would it be better described by two linear relations, with a break radius at corotation radius (Bresolin et al. 2012, and references therein) or further out (Donor et al. 2020) or a more sophisticated function (see e.g. Chiappini et al. 2001; Kubryk et al. 2015)? Investigating the gradient's form helps in understanding the galactic processes influencing metallicity at different radii (Minchev et al. 2014).

SB: "However, a simple, linear gradient may not be the better way to describe the distribution of the elements in the Galactic disk. From Cepheids, Andrievsky et al. (2002b), Pedicelli et al. (2009, 2010), and Genovali et al. (2013) found a steeper gradient in the very inner disk (≤ 7 kpc)." from Lemasle et al. (2013)

SB: "There are numerous abundance studies of open clusters from different groups: [...] They all reach the same conclusion: a linear gradient of approximately −0.06 dex/kpc extending quite far into the outer disk, and a flattening at a level of [Fe/H] ≈ −0.3 dex, somewhere between 10 and 14 kpc." from Lemasle et al. (2013).

SB: Lemasle et al. (2008) find $\mathrm{d[Fe/H]}/\mathrm{d}R = -0.050 \pm 0.008\,\mathrm{dex\,kpc^{-1}}$ in the 5-17 kpc range, but $\mathrm{d[Fe/H]}/\mathrm{d}R = -0.012 \pm 0.014\,\mathrm{dex\,kpc^{-1}}$ in a smaller 10-15 kpc range.

SB: Put some of these results into context of the Milky Way in Fig. 10.

4.2 Scatter in the gradient

How much scatter in the radial metallicity gradient of young stars is expected based on simulations? Quantifying the scatter can provide

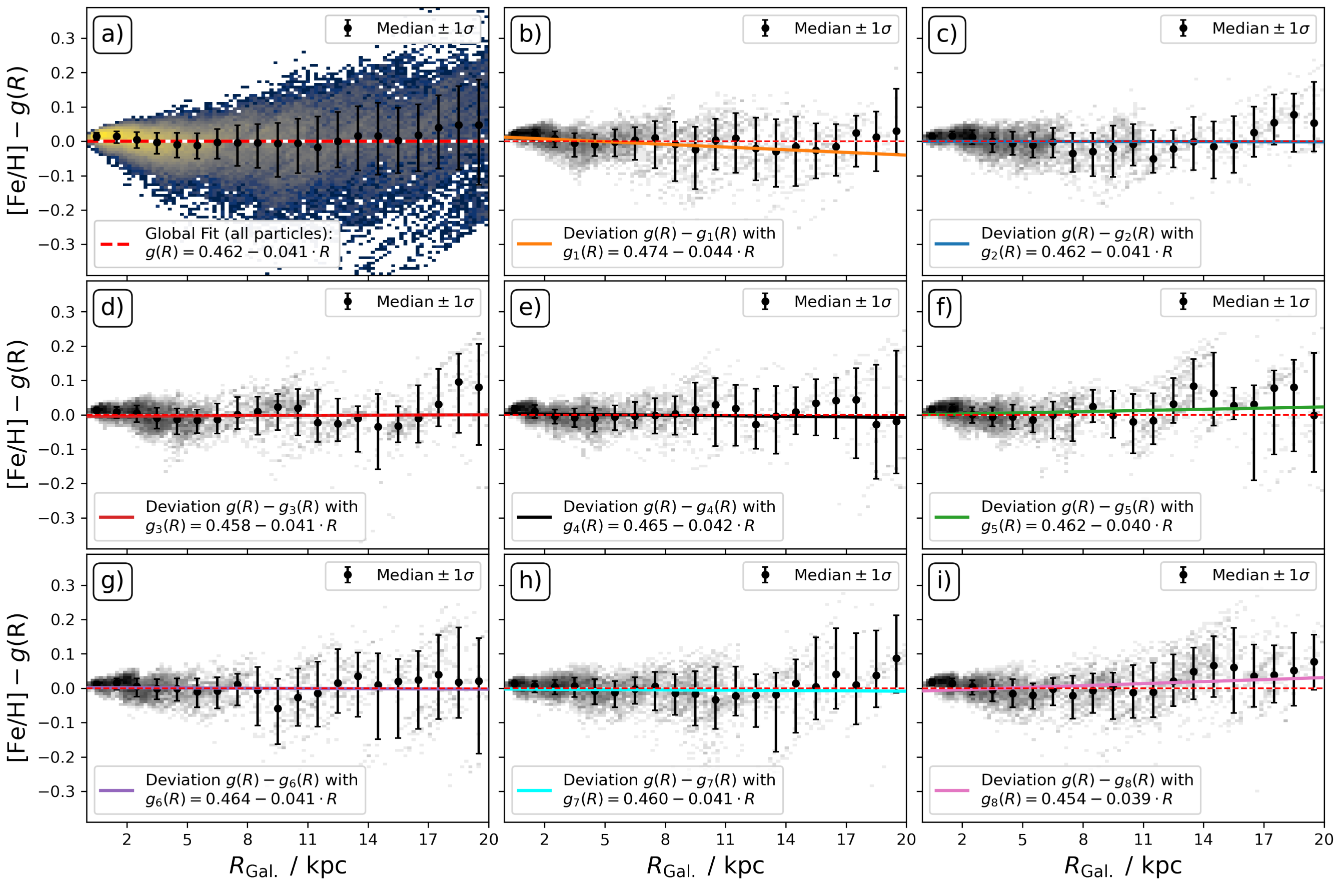

Figure 8. Density variation of the radial metallicity gradient R – [Fe/H] across full stellar disk (panel a) and 8 different sectors (same panel order as for Fig. 7). Linear radial metallicity gradients have been fit globally (red dashed line) and for each sector with colors following the same color code as in Fig. 7.

insights into the effects of transient events like mergers, star formation bursts, and gas accretion.

•

SB: Put some of these results into context of the Milky Way in Fig. 11, e.g. Poggio et al. (2021) and Hackshaw et al. (2024).

4.3 Coherence of the gradient with position

How significant is the change in the radial metallicity of young stars gradient as a function of position, both in terms of radial coverage and azimuth? Understanding these variations can reveal the underlying processes affecting metallicity distribution, such as spiral arm dynamics and bar-driven mixing (see their Figs. 5-8 Di Matteo et al. 2013).

4.4 Coherence of the gradient with age

Until what stellar age can stars be used as reliable tracers of the gas disk in simulations, in terms of both chemical composition and position? This question is pivotal for interpreting observed gradients across different ages (e.g. Willett et al. 2023) and comparing them with model predictions, particularly concerning the migration and heating of stellar populations (Binney & Tremaine 2008; Frankel et al. 2018).

4.5 Application of quadratic gradient function onto observations

- Can we apply our functional form onto MW data? e.g. Genovali et al. (2014)?
- Can we apply our functional form onto extragalactic data? e.g. Chen et al. (2023)?

5 CONCLUSIONS

5.1 Main Take-Away

5.2 Future Research

- Can we say what the linear gradient and flattening part is for $R_{\rm eff}$ for our NIHAO Milky Way analogue. Can we relate this to the MW effective radius and other galaxies?

ACKNOWLEDGEMENTS

We acknowledge the traditional owners of the land on which the AAT and ANU stand, the Gamilaraay, the Ngunnawal and Ngambri people. We pay our respects to elders past, present, and emerging and are proud to continue their tradition of surveying the night sky in the Southern hemisphere.

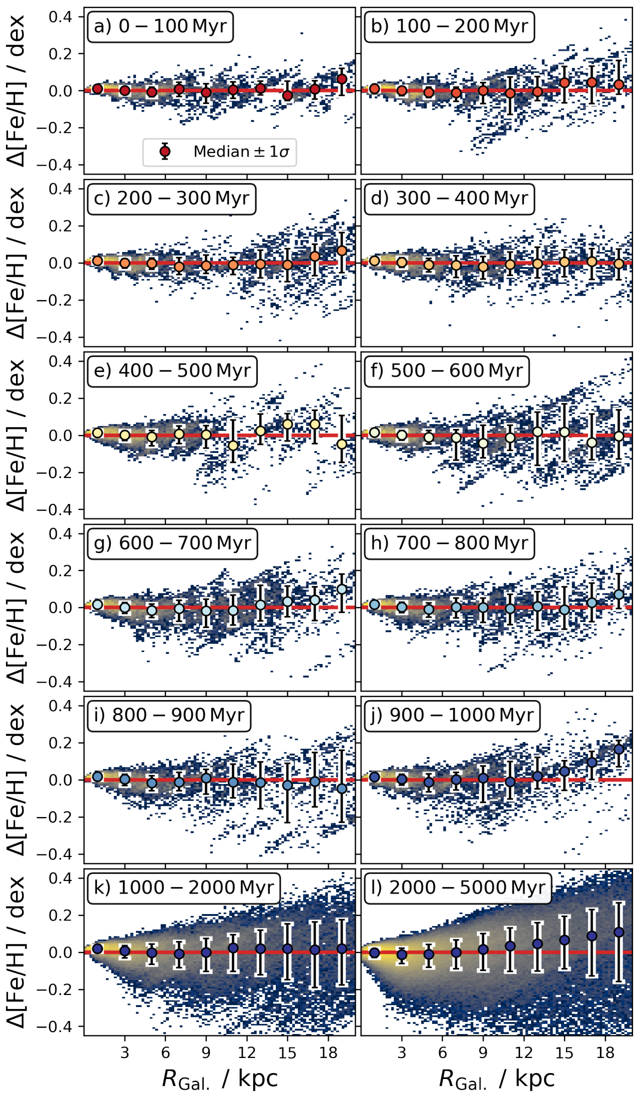

Figure 9. Density distribution and spread of [Fe/H] across different galactocentric radii with respect to a global linear radial metallicity gradient across different age ranges. Panels a-j) show young stars and exhibit a rather similar trend, whereas the scatter increases significantly for stars above 1 Gyr in panels panels k) and l).

This work was supported by the Australian Research Council Centre of Excellence for All Sky Astrophysics in 3 Dimensions (ASTRO 3D), through project number CE170100013. SB acknowledges support from the Australian Research Council under grant number DE240100150 which enabled SB to continue researching at the end of a fixed-term position and finalising this study. TB acknowledges funding from the Carl Zeiss Stiftung and support from the European Research Council under ERC-CoG grant CRAGSMAN-646955. We gratefully acknowledge the Gauss Centre for Supercomputing e.V. (`www.gauss-centre.eu`) for funding this project by providing computing time on the GCS Supercomputer SuperMUC at Leibniz Supercomputing Centre (`www.lrz.de`). Simulations were partially computed with High Performance Computing resources at New York University, Abu Dhabi.

FACILITIES

AAT with 2df-HERMES at Siding Spring Observatory: The GALAH Survey is based data acquired through the Australian Astronomical Observatory, under programs: A/2013B/13 (The GALAH pilot survey); A/2014A/25, A/2015A/19, A2017A/18 (The GALAH survey phase 1), A2018 A/18 (Open clusters with HERMES), A2019A/1 (Hierarchical star formation in Ori OB1), A2019A/15 (The GALAH survey phase 2), A/2015B/19, A/2016A/22, A/2016B/10, A/2017B/16, A/2018B/15 (The HERMES-TESS program), and A/2015A/3, A/2015B/1, A/2015B/19, A/2016A/22, A/2016B/12, A/2017A/14, (The HERMES K2-follow-up program). This paper includes data that has been provided by AAO Data Central (`datacentral.aao.gov.au`).

***Gaia*:** This work has made use of data from the European Space Agency (ESA) mission *Gaia* (`http://www.cosmos.esa.int/gaia`), processed by the *Gaia* Data Processing and Analysis Consortium (DPAC, `http://www.cosmos.esa.int/web/gaia/dpac/consortium`). Funding for the DPAC has been provided by national institutions, in particular the institutions participating in the *Gaia* Multilateral Agreement.

Other facilities: This publication makes use of data products from the Two Micron All Sky Survey (Skrutskie et al. 2006) and the CDS VizieR catalogue access tool (Ochsenbein et al. 2000).

SOFTWARE

The research for this publication was coded in PYTHON (version 3.7.4) and included its packages ASTROPY (v. 3.2.2; Astropy Collaboration et al. 2013, 2018), IPYTHON (v. 7.8.0; Pérez & Granger 2007), MATPLOTLIB (v. 3.1.3; Hunter 2007), NUMPY (v. 1.17.2; Walt et al. 2011), PYNBODY (v. 1.1.0; Pontzen et al. 2013), SCIPY (v. 1.3.1; Virtanen et al. 2020), SKLEARN (v. 1.5.1 Pedregosa et al. 2011) STATSMODELS (v. 0.14.2 Perktold et al. 2024) We further made use of TOPCAT (version 4.7; Taylor 2005);

DATA AVAILABILITY

All code and data to reproduce the analysis and figures can be accessed via `https://github.com/svenbuder/age_abundance_nihao_vs_galah`.

REFERENCES

Agertz O., et al., 2021, MNRAS, 503, 5826
Allende Prieto C., Beers T. C., Wilhelm R., Newberg H. J., Rockosi C. M., Yanny B., Lee Y. S., 2006, ApJ, 636, 804
Anders F., et al., 2014, A&A, 564, A115
Anders F., et al., 2017, A&A, 600, A70
Andrievsky S. M., et al., 2002a, A&A, 381, 32
Andrievsky S. M., Bersier D., Kovtyukh V. V., Luck R. E., Maciel W. J., Lépine J. R. D., Beletsky Y. V., 2002b, A&A, 384, 140
Astropy Collaboration et al., 2013, A&A, 558, A33
Astropy Collaboration et al., 2018, AJ, 156, 123
Bellardini M. A., Wetzel A., Loebman S. R., Faucher-Giguère C.-A., Ma X., Feldmann R., 2021, MNRAS, 505, 4586
Bellardini M. A., Wetzel A., Loebman S. R., Bailin J., 2022, MNRAS, 514, 4270
Bergemann M., et al., 2014, A&A, 565, A89
Binney J., Tremaine S., 2008, Galactic Dynamics: Second Edition. Princeton University Press
Boeche C., et al., 2013, A&A, 559, A59

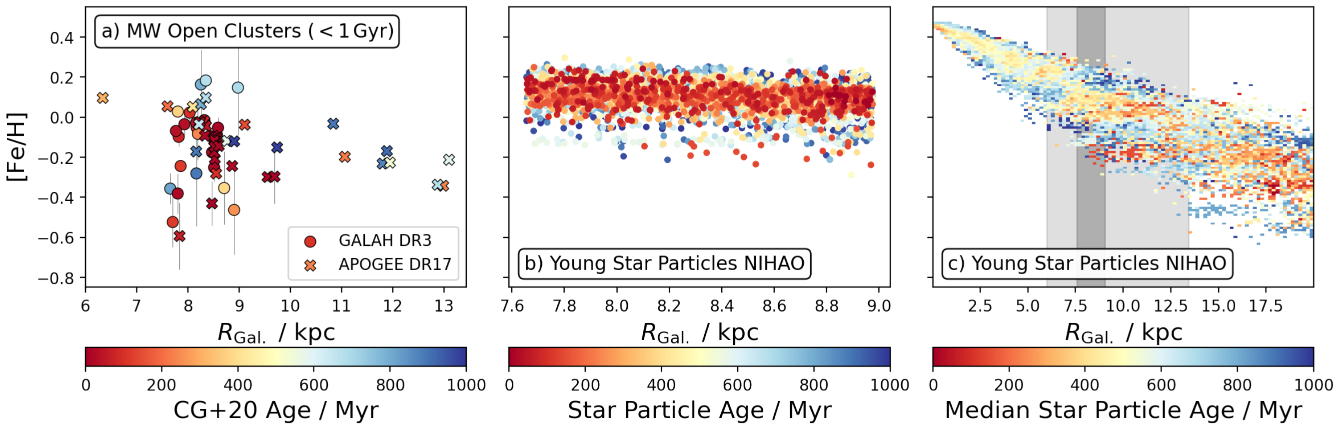

Figure 10. Caption

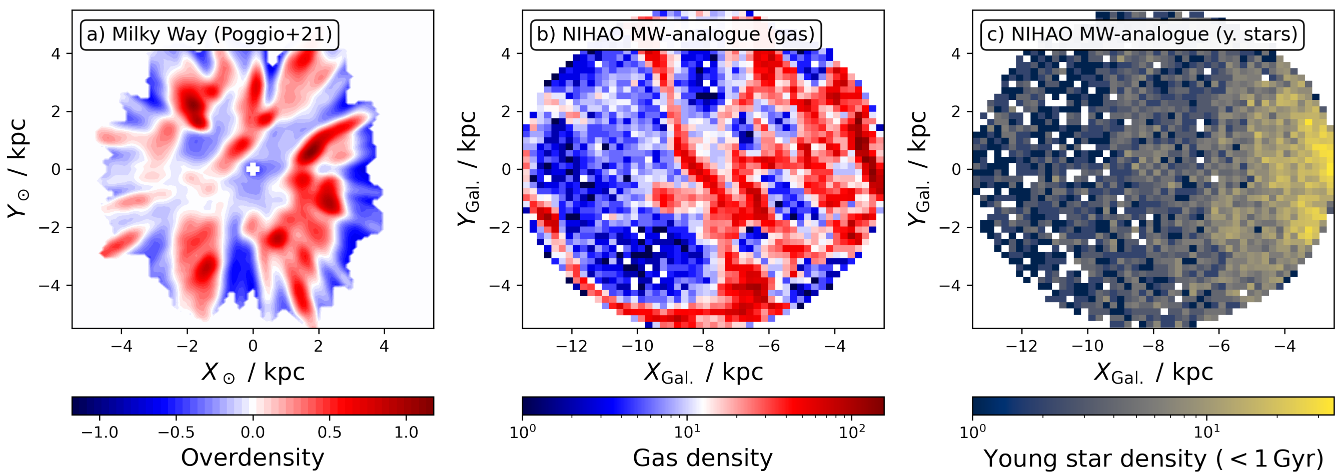

Figure 11. Caption

Bresolin F., Kennicutt R. C., Ryan-Weber E., 2012, ApJ, 750, 122
Buck T., Obreja A., Macciò A. V., Minchev I., Dutton A. A., Ostriker J. P., 2020, MNRAS, 491, 3461
Buck T., Rybizki J., Buder S., Obreja A., Macciò A. V., Pfrommer C., Steinmetz M., Ness M., 2021, MNRAS, 508, 3365
Buder S., Mijnarends L., Buck T., 2024, MNRAS, 532, 1010
Casamiquela L., et al., 2019, MNRAS, 490, 1821
Chabrier G., 2003, PASP, 115, 763
Chen Q.-H., Grasha K., Battisti A. J., Kewley L. J., Madore B. F., Seibert M., Rich J. A., Beaton R. L., 2023, MNRAS, 519, 4801
Chen Q.-H., et al., 2024, MNRAS, 527, 2991
Chiappini C., 2002, Ap&SS, 281, 253
Chiappini C., Matteucci F., Romano D., 2001, ApJ, 554, 1044
Chiosi C., 1980, A&A, 83, 206
Cunha K., et al., 2016, Astronomische Nachrichten, 337, 922
Di Matteo P., Haywood M., Combes F., Semelin B., Snaith O. N., 2013, A&A, 553, A102
Donor J., et al., 2020, AJ, 159, 199
Frankel N., Rix H.-W., Ting Y.-S., Ness M., Hogg D. W., 2018, ApJ, 865, 96
Frankel N., Sanders J., Ting Y.-S., Rix H.-W., 2020, arXiv e-prints, p. arXiv:2002.04622
Gaia Collaboration et al., 2016, A&A, 595, A1
Genovali K., et al., 2014, A&A, 566, A37
Graf R. L., Wetzel A., Bellardini M. A., Bailin J., 2024, arXiv e-prints, p. arXiv:2402.15614
Grand R. J. J., Kawata D., Cropper M., 2015, MNRAS, 447, 4018
Hackshaw Z., Hawkins K., Filion C., Horta D., Laporte C. F. P., Carr C., Price-Whelan A. M., 2024, arXiv e-prints, p. arXiv:2405.18120
Hayden M. R., et al., 2014, AJ, 147, 116
Hayden M. R., et al., 2015, ApJ, 808, 132
Hogg D. W., Eilers A.-C., Rix H.-W., 2019, AJ, 158, 147
Hunter J. D., 2007, Comput Sci Eng, 9, 90
Imig J., et al., 2023, ApJ, 954, 124
Janes K. A., 1979, ApJS, 39, 135
Karakas A. I., Lugaro M., 2016, ApJ, 825, 26
Katz D., Soubiran C., Cayrel R., Barbuy B., Friel E., Bienaymé O., Perrin M. N., 2011, A&A, 525, A90
Khoperskov S., Sivkova E., Saburova A., Vasiliev E., Shustov B., Minchev I., Walcher C. J., 2023, A&A, 671, A56
Knollmann S. R., Knebe A., 2009, ApJS, 182, 608
Kubryk M., Prantzos N., Athanassoula E., 2015, A&A, 580, A126
Larson R. B., 1976, MNRAS, 176, 31
Lemasle B., François P., Bono G., Mottini M., Primas F., Romaniello M., 2007, A&A, 467, 283
Lemasle B., François P., Piersimoni A., Pedicelli S., Bono G., Laney C. D., Primas F., Romaniello M., 2008, A&A, 490, 613

Lemasle B., et al., 2013, A&A, 558, A31
Lemasle B., et al., 2022, A&A, 668, A40
Limongi M., Chieffi A., 2018, ApJS, 237, 13
Ma X., Hopkins P. F., Wetzel A. R., Kirby E. N., Anglés-Alcázar D., Faucher-Giguère C.-A., Kereš D., Quataert E., 2017, MNRAS, 467, 2430
Magrini L., et al., 2017, A&A, 603, A2
Matteucci F., ed. 2001, The chemical evolution of the Galaxy Astrophysics and Space Science Library Vol. 253, doi:10.1007/978-94-010-0967-6.
Metha B., Trenti M., Chu T., 2021, MNRAS, 508, 489
Minchev I., Chiappini C., Martig M., 2014, A&A, 572, A92
Mun M., et al., 2024, MNRAS, 530, 5072
Myers N., et al., 2022, AJ, 164, 85
Ochsenbein F., Bauer P., Marcout J., 2000, A&AS, 143, 23
Pedregosa F., et al., 2011, J Mach Learn Res, 12, 2825
Pérez F., Granger B. E., 2007, Comput Sci Eng, 9, 21
Perktold J., et al., 2024, statsmodels/statsmodels: Release 0.14.2, doi:10.5281/zenodo.593847
Pilkington K., et al., 2012, A&A, 540, A56
Planck Collaboration et al., 2014, A&A, 571, A16
Poggio E., et al., 2018, MNRAS, 481, L21
Poggio E., et al., 2021, A&A, 651, A104
Poggio E., et al., 2022, A&A, 666, L4
Pontzen A., Roškar R., Stinson G. S., Woods R., 2013, pynbody: Astrophysics Simulation Analysis for Python, Astrophysics Source Code Library, record ascl:1305.002
Rolleston W. R. J., Smartt S. J., Dufton P. L., Ryans R. S. I., 2000, A&A, 363, 537
Rybizki J., Just A., Rix H.-W., 2017, A&A, 605, A59
Sánchez S. F., et al., 2014, A&A, 563, A49
Searle L., 1971, ApJ, 168, 327
Seitenzahl I. R., et al., 2013, MNRAS, 429, 1156
Shaver P. A., McGee R. X., Newton L. M., Danks A. C., Pottasch S. R., 1983, MNRAS, 204, 53
Skrutskie M. F., et al., 2006, AJ, 131, 1163
Spina L., et al., 2021, MNRAS, 503, 3279
Stanghellini L., Magrini L., Casasola V., 2015, ApJ, 812, 39
Stinson G., Seth A., Katz N., Wadsley J., Governato F., Quinn T., 2006, MNRAS, 373, 1074
Stinson G. S., Brook C., Macciò A. V., Wadsley J., Quinn T. R., Couchman H. M. P., 2013, MNRAS, 428, 129
Taylor M. B., 2005, ASPC, 347, 29
Tinsley B. M., 1980, Fundamentals Cosmic Phys., 5, 287
Tissera P. B., Rosas-Guevara Y., Bower R. G., Crain R. A., del P Lagos C., Schaller M., Schaye J., Theuns T., 2019, MNRAS, 482, 2208
Twarog B. A., 1980, ApJ, 242, 242
Twarog B. A., Ashman K. M., Anthony-Twarog B. J., 1997, AJ, 114, 2556
Vickers J. J., Shen J., Li Z.-Y., 2021, ApJ, 922, 189
Vilchez J. M., Esteban C., 1996, MNRAS, 280, 720
Virtanen P., et al., 2020, Nature Methods, 17, 261
Wadsley J. W., Keller B. W., Quinn T. R., 2017, MNRAS, 471, 2357
Walt S. v. d., Colbert S. C., Varoquaux G., 2011, Comput Sci Eng, 13, 22
Wang L., Dutton A. A., Stinson G. S., Macciò A. V., Penzo C., Kang X., Keller B. W., Wadsley J., 2015, MNRAS, 454, 83
Willett E., et al., 2023, MNRAS, 526, 2141
Zari E., Hashemi H., Brown A. G. A., Jardine K., de Zeeuw P. T., 2018, A&A, 620, A172
Zari E., Rix H. W., Frankel N., Xiang M., Poggio E., Drimmel R., Tkachenko A., 2021, A&A, 650, A112

This paper has been typeset from a TEX/LATEX file prepared by the author.